High-frequency dominant depression of peripheral vagal control of heart rate in rats with chronic heart failure

T. Kawada,[1] M. Li,[1] S. Shimizu,[1] A. Kamiya,[1] K. Uemura,[1] M. J. Turner,[1] M. Mizuno[2] and M. Sugimachi[1]

1 Department of Cardiovascular Dynamics, National Cerebral and Cardiovascular Center, Osaka, Japan

2 Department of Health Care Sciences, University of Texas Southwestern Medical Center, Dallas, TX, USA

Received 2 November 2012,
revision requested 2 December 2012,
revision received 5 December 2012,
accepted 15 December 2012
Correspondence: T. Kawada, MD, PhD, Department of Cardiovascular Dynamics, National Cerebral and Cardiovascular Center Research Institute, 5-7-1 Fujishirodai, Suita, Osaka 565-8565, Japan.
E-mail: torukawa@ri.ncvc.go.jp

Abstract

Aim: To examine whether dynamic characteristics of the peripheral vagal control of heart rate (HR) are altered in chronic heart failure (CHF).

Methods: The right vagal nerve was electrically stimulated according to a binary white noise signal, and the transfer function from vagal nerve stimulation (VNS) to HR was estimated in the frequency range from 0.01 to 1 Hz in five control rats and five CHF rats under anaesthetized conditions. The rate of VNS was changed among 10, 20 and 40 Hz.

Results: A multiple linear regression analysis indicated that the increase in the VNS rate augmented the ratio of the high-frequency (HF) gain to the steady-state gain in the control group but not in the CHF group. As a result, the dynamic gain of the transfer function in the frequencies near 1 Hz decreased more in the CHF group than in the control group.

Conclusion: Changes in the dynamic characteristics of the peripheral vagal control of HR may contribute to the manifestation of decreased HF components of HR variability observed in CHF.

Keywords transfer function, vagal nerve stimulation, white noise analysis.

Heart rate (HR) is mainly governed by the autonomic nervous system. The dynamic HR response to autonomic nervous activity is important for moment-to-moment adjustments of cardiac function during daily activity. High-frequency (HF) components of HR variability (HRV) are considered to be an index of vagal nerve activity, because the dynamic HR response to vagal nerve activity is faster than that to sympathetic nerve activity (Akselrod *et al.* 1981, Berger *et al.* 1989, Kawada *et al.* 1996, Mizuno *et al.* 2010). The HF components of HRV are known to be decreased in diseased conditions such as chronic heart failure (CHF; Task Force of the European Society of Cardiology 1996, Olshansky *et al.* 2008). The interpretation of the HF components can depend on the input–output transduction property from vagal nerve activity to HR. For instance, the decreased HF components may indicate diminished vagal outflow from the central nervous system if the transduction property is not changed between normal and CHF conditions. On the other hand, there is also a possibility that the decreased HF components are merely the result of impaired transduction property from vagal nerve activity to HR in the HF range. To better understand the significance of the decreased HF components of HRV observed in CHF, quantification of the transduction property becomes essential.

The input–output transduction property of a biological system usually reveals dynamic characteristics (Sagawa 1983). That is to say, the amplitude and the phase lag of the system response vary depending on the frequency of the input modulation. In the case of the vagal control of HR, the transduction property has low-pass characteristics (Berger *et al.* 1989, Kawada *et al.* 1996, Mizuno *et al.* 2010). The amplitude of the HR response is large when the frequency of vagal modulation is low, and the amplitude of the HR response becomes smaller as the frequency of vagal

modulation increases. It remains unknown, however, whether the dynamic characteristics of the peripheral vagal control of HR are altered in CHF. To test the hypothesis that dynamic characteristics of the peripheral vagal control of HR are altered in CHF, the transfer functions from efferent vagal nerve stimulation (VNS) to HR were compared between normal control rats and rats with CHF following myocardial infarction.

Materials and methods

The study is conform with Good Publishing Practice in Physiology (Persson & Henriksson 2011). Experiments were performed on adult male Sprague–Dawley rats.

CHF rats

Myocardial infarction was induced under halothane anaesthesia by ligating the left coronary artery in 8-week-old rats according to a previously established procedure (Li *et al.* 2004, Kawada *et al.* 2010). After recovered from the anaesthesia, the rats were fed with standard laboratory chow *ad libitum* and with free access to water. Rats that survived for 8 weeks after myocardial infarction were used for the CHF group.

Animal preparation

Rats were anaesthetized with an intraperitoneal injection (2 mL kg^{-1}) of a mixture of urethane (250 mg mL^{-1}) and α-chloralose (40 mg mL^{-1}), followed by a maintenance dose of intravenous continuous infusion of the anaesthetic mixture. The trachea was intubated and artificial ventilation was performed. An arterial catheter was inserted into the right femoral artery to monitor arterial pressure. A body surface electrocardiogram was recorded, and HR was detected through use of a cardiotachometer.

To avoid a possible contribution from reflexes arising from cardiopulmonary regions and aortic arch, the vagi and the aortic depressor nerves were sectioned at the neck. To minimize reflex changes in efferent sympathetic nerve activity, bilateral carotid sinuses were isolated from the systemic circulation (Shoukas *et al.* 1991, Sato *et al.* 1999, Kawada *et al.* 2010), and intracarotid sinus pressure was held at 120 mmHg during VNS.

A pair of stainless steel wire electrodes (Bioflex wire, AS633; Cooner Wire, Chatsworth, CA, USA) was attached to the sectioned distal end of the right cervical vagus for efferent VNS. The nerve and electrodes were secured and insulated with silicone glue (Kwik-Sil; World Precision Instruments, Sarasota, FL, USA). The pulse duration was set to 2 ms. The pulse amplitude was set to supramaximal in each rat using 10-Hz constant VNS so that increasing the amplitude did not further decrease HR. The resultant amplitude ranged from 2.0 to 3.5 V.

Protocols

In five control rats and five CHF rats, VNS was turned on and off every 500 ms according to a binary white noise signal. The input power spectrum of VNS was reasonably constant up to 1 Hz, and the transfer function from VNS to HR was estimated up to 1 Hz. Three intensities of VNS (10, 20 and 40 Hz) were tested in random order in each rat. To avoid possible confusion in later transfer function descriptions, VNS frequency will hereafter be referred to as the VNS rate. The binary white noise input using each VNS rate was applied for 15 min.

Data analysis

Data were sampled at 1000 Hz using a 16-bit analogue-to-digital converter and stored on a dedicated laboratory computer system. The transfer function from VNS to HR was estimated by treating VNS as the system input perturbation and HR as the system output response (Mizuno *et al.* 2010). The coherence was also calculated as an index of linear dependence of the system output on the input perturbation. The coherence takes values from zero to unity. Zero coherence indicates total independence between the input and output signals. Unity coherence indicates that the output was perfectly explained by linear dynamics of the input.

Transfer function model

While we previously used a first-order low-pass filter with pure dead time to describe the transfer function from VNS to HR in rabbits (Kawada *et al.* 1996, Nakahara *et al.* 1998, Miyamoto *et al.* 2004, Mizuno *et al.* 2007), this model was not necessarily the best model to describe the transfer function from VNS to HR in rats (Mizuno *et al.* 2010). To better describe the estimated transfer function in rats, we employed a following new model (Kawada *et al.* 2012):

$$H(f) = -K\left(\frac{1-R}{1+\frac{f}{f_C}j}+R\right)e^{-2\pi fLj}$$

where j denotes the imaginary units; K (in bpm Hz^{-1}) is the steady-state gain which is an asymptote of dynamic gain of $H(f)$ as the frequency tends to zero; f_C (in Hz) is the corner frequency corresponding to a first-order low-pass filter; L (in s) is the pure dead

time; and R (no units) is the ratio of the HF gain to the steady-state gain. As the frequency increases beyond the corner frequency toward infinity, the dynamic gain of $H(f)$ asymptotically approaches KR. When R equals zero, $H(f)$ reduces to a simple first-order low-pass filter with pure dead time used in the previous studies. Hereafter in this study, R is referred to as 'relative HF gain'.

Statistical analysis

All data are presented as mean ± SE. Differences in transfer function parameters were analysed by a multiple linear regression as follows (Glantz & Slinker 2001):

$$p = C + B_{VNS} \times D_{VNS} + B_{CHF} \times D_{CHF} + B_{Interaction} \times D_{VNS} \times D_{CHF} + B_{m1} \times D_{m1} + \cdots + B_{m4} \times D_{m4} + B_{n1} \times D_{n1} + \cdots + B_{n4} \times D_{n4}$$

where p represents each parameter value; C is a constant term or an intercept of the multiple linear regression; B_{VNS} is a coefficient for the VNS effect; D_{VNS} is a dummy variable encoding the VNS rate ($D_{VNS} = 0$ for 10 Hz, $D_{VNS} = 1$ for 20 Hz, and $D_{VNS} = 2$ for 40 Hz); B_{CHF} is a coefficient for the CHF effect; D_{CHF} is a dummy variable encoding the CHF animals ($D_{CHF} = 0$ for the control rats, and $D_{CHF} = 1$ for the CHF rats); $B_{Interaction}$ is a coefficient for the interaction effect between D_{VNS} and D_{CHF}; D_{m1} through D_{m4} are dummy variables encoding five different animals in the control group; D_{n1} through D_{n4} are dummy variables encoding five different animals in the CHF group (see Table 1); and B_{m1} through B_{m4} and B_{n1} through B_{n4} are coefficients for inter-individual variations. Note that C is an estimate of the parameter value corresponding to the transfer function obtained by 10-Hz VNS ($D_{VNS} = 0$) in the control group ($D_{CHF} = 0$). B_{VNS}, B_{CHF}, and $B_{Interaction}$ were tested as to whether they were significantly different from zero, with a significance level set at $P < 0.05$ (Glantz & Slinker 2001).

Table 1 Dummy variables encoding experimental animals

	D_{m1}	D_{m2}	D_{m3}	D_{m4}	D_{n1}	D_{n2}	D_{n3}	D_{n4}
Control no. 1	1	0	0	0	0	0	0	0
Control no. 2	0	1	0	0	0	0	0	0
Control no. 3	0	0	1	0	0	0	0	0
Control no. 4	0	0	0	1	0	0	0	0
Control no. 5	−1	−1	−1	−1	0	0	0	0
CHF no. 1	0	0	0	0	1	0	0	0
CHF no. 2	0	0	0	0	0	1	0	0
CHF no. 3	0	0	0	0	0	0	1	0
CHF no. 4	0	0	0	0	0	0	0	1
CHF no. 5	0	0	0	0	−1	−1	−1	−1

To encode five different animals, four dummy variables are needed in each group. The encoding does not cross the boundary between the control and chronic heart failure (CHF) groups. Effects coding was used to model the inter-individual differences (Glantz & Slinker 2001).

Results

Figure 1 represents typical results obtained from a control rat. Dynamic HR responses to the binary white noise inputs using 10, 20 and 40-Hz VNS are shown in Figure 1a. After the onset of VNS, HR decreased intermittently in response to the binary VNS. As the VNS rate increased, the magnitude of dynamic HR response increased. The group-averaged decreases in mean HR relative to the pre-stimulation HR were 54 ± 4, 84 ± 14 and 137 ± 17 bpm (13 ± 1, 19 ± 3, and 32 ± 3%) during 10, 20 and 40-Hz VNS respectively. Transfer functions from VNS to HR are depicted in Figure 1b. The solid lines are the calculated transfer functions, and the grey smooth lines are the corresponding model transfer functions. The dynamic gain became smaller as the frequency increased during 10-Hz VNS, indicating low-pass characteristics of the system. The dynamic gain, however, did not fall off smoothly during 20-Hz VNS, and the gain plot exhibited a plateau in the frequencies above 0.3 Hz. The gain plot became much flatter during 40-Hz VNS. The phase approached $-\pi$ radians at the lowest frequency, reflecting the negative HR response to VNS. The coherence was close to unity in the frequencies below 0.1 Hz and decreased slightly in the frequencies above 0.1 Hz.

Figure 2 shows typical results obtained from a CHF rat. The magnitudes of dynamic HR responses to binary VNS were smaller than those in the control rat (Figs 2a vs. 1a). The rapid restorations of HR to baseline HR were not observed during 20- and 40-Hz VNS in the CHF rat. The group-averaged decreases in mean HR relative to the pre-stimulation HR were 46 ± 8, 71 ± 12 and 157 ± 24 bpm (12 ± 2, 18 ± 3 and 38 ± 6%) during 10, 20 and 40-Hz VNS respectively. The transfer function from VNS to HR

Acta Physiologica © 2012 Scandinavian Physiological Society, doi: 10.1111/apha.12055

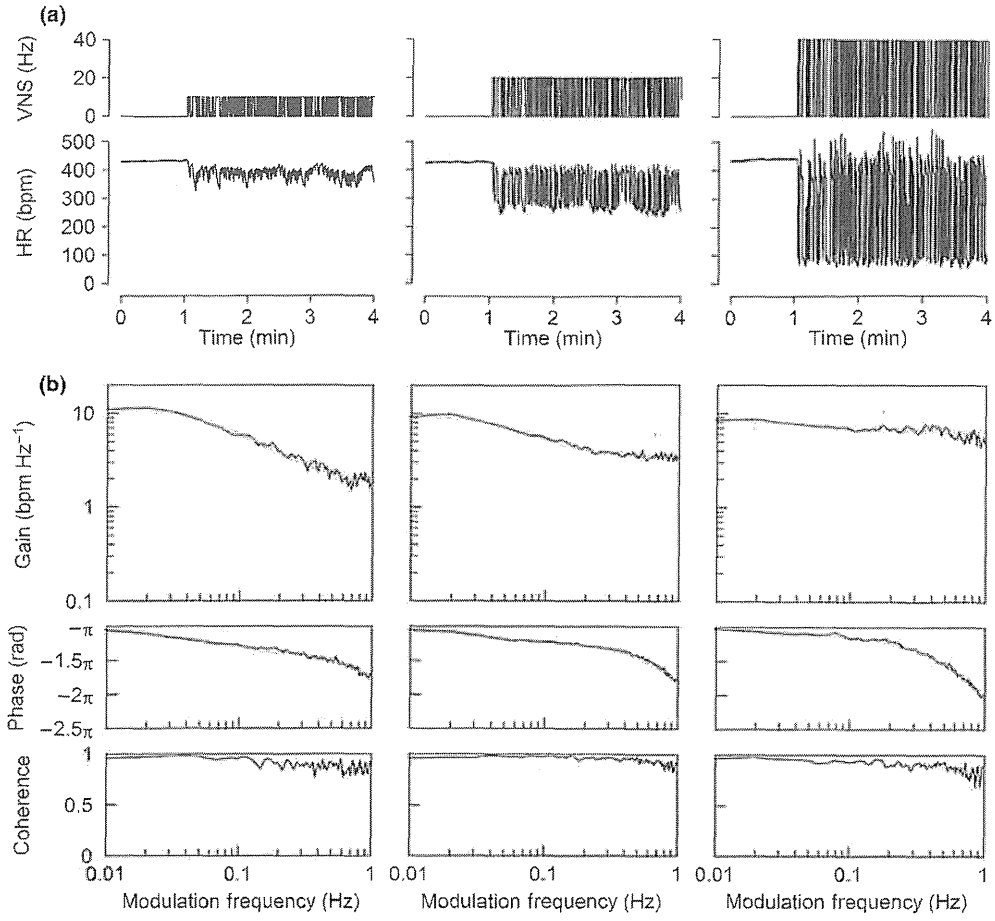

Figure 1 (a) Typical experimental data showing the binary white noise input using vagal nerve stimulation (VNS) and corresponding heart rate (HR) response in a control rat. The VNS rate was changed among 10, 20 and 40 Hz. (b) Transfer functions from VNS to HR corresponding to the time series data. The thin black lines indicate the estimated transfer functions. The bold grey lines indicate the fitting results of the model transfer functions.

revealed low-pass characteristics in the CHF rat (Fig. 2b). In contrast to the normal rat, the increase in the VNS rate did not manifest a plateau of the dynamic gain in the higher frequency range. The phase approached $-\pi$ radians at the lowest frequency and delayed smoothly as the frequency increased. The coherence was close to unity during 10-Hz VNS. There were decreases in coherence in the frequencies above 0.4 Hz during 20-Hz VNS. The coherence became lower during 40-Hz VNS compared to that during 20-Hz VNS.

Figure 3 depicts group-averaged transfer functions. The shape of the transfer function during 10-Hz VNS was similar between the control and CHF groups, except for a nearly parallel downward shift in the gain plot in the CHF group. The shape of the transfer function during 20-Hz VNS differed between the control and CHF groups in that there was a plateau in the gain plot above 0.5 Hz in the control group. The plateau in the gain plot became more overt and occurred above 0.3 Hz during 40-Hz VNS in the control group. The relative HF gain in the model transfer function is frequency independent, which means that the increase in the relative HF gain reduces the phase delay (Fig. 4b, middle). As can be seen in Figure 3, the magnitudes of phase delay from $-\pi$ radians in the higher frequency range were smaller in the control group compared to the CHF group during 20 and 40-Hz VNS. The results of the multiple linear regression analysis on the transfer function parameters are summarized in Table 2.

Discussion

Although HF components of HRV are known to be decreased in CHF (Task Force of the European Society of Cardiology 1996, Olshansky *et al.* 2008), the present study is the first to demonstrate changes in the dynamic characteristics of the peripheral vagal control of HR in CHF.

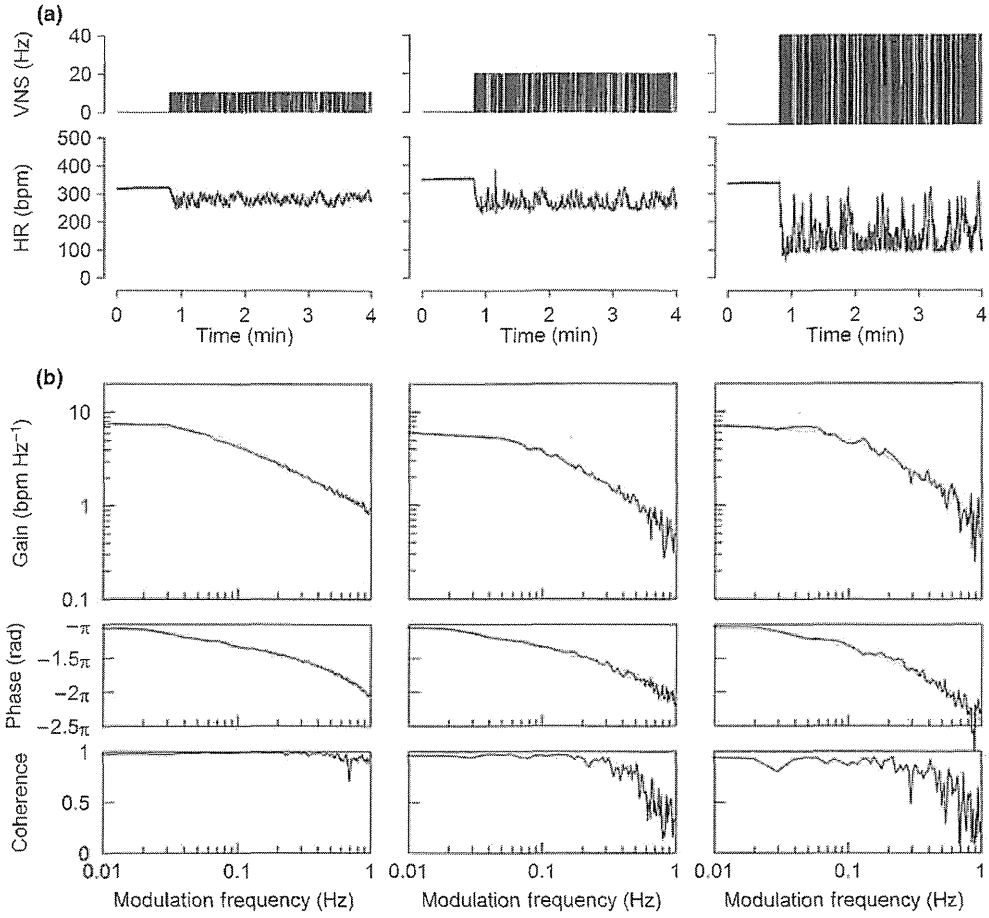

Figure 2 (a) Typical experimental data showing the binary white noise input using vagal nerve stimulation (VNS) and corresponding heart rate (HR) response in a rat with chronic heart failure. The VNS rate was changed among 10, 20 and 40 Hz. (b) Transfer functions from VNS to HR corresponding to the time series data. The thin black lines indicate the estimated transfer functions. The bold grey lines indicate the fitting results of the model transfer functions.

Effects of CHF and VNS rate on the steady-state gain

The steady-state gain, K, determines vertical location of the transduction property in the gain plot (Fig. 4a, top) without influencing the phase plot (Fig. 4a, middle). An increase in the steady-state gain is associated with an augmented step response of HR (Fig. 4a, bottom). The effect of CHF (B_{CHF}) on the steady-state gain was significantly negative (Table 2), suggesting overall depression of the peripheral vagal control of HR in the CHF group compared to the control group. Several factors are considered to attenuate the HR response to VNS as follows. Bibevski & Dunlap (1999) have suggested that parasympathetic ganglionic transmission is attenuated in heart failure. Angiotensin II, which is known to be increased in CHF conditions (Riegger 1985), attenuates myocardial interstitial acetylcholine release in response to VNS (Kawada *et al.* 2007) and reduces the dynamic gain of the transfer function from VNS to HR (Kawada *et al.* 2009). Du *et al.* (1998) demonstrated that blockade of angiotensin II type 1 receptors by losartan-enhanced bradycardia induced by VNS in rats with chronic myocardial infarction. Besides the effect of CHF, the effect of VNS rate (B_{VNS}) on the steady-state gain was also significantly negative, suggesting that the HR response became saturated and did not increase in proportion to the increased VNS rate. The decrease in the steady-state gain at higher VNS rates is consistent with the study by Berger *et al.* (1989) where the canine atrial response was examined.

Interactions exist between the sympathetic and parasympathetic nervous systems in regulating HR. In a presynaptic mechanism, noradrenaline released from the sympathetic nerve endings inhibits acetylcholine release from the vagal nerve endings through α_1-adrenergic receptors (Wetzel *et al.* 1985). In a postsynaptic mechanism, accumulation of cyclic AMP in the sinus nodal cells by β-adrenergic stimulation augments the dynamic vagal control of HR (Nakahara *et al.* 1998). Levy

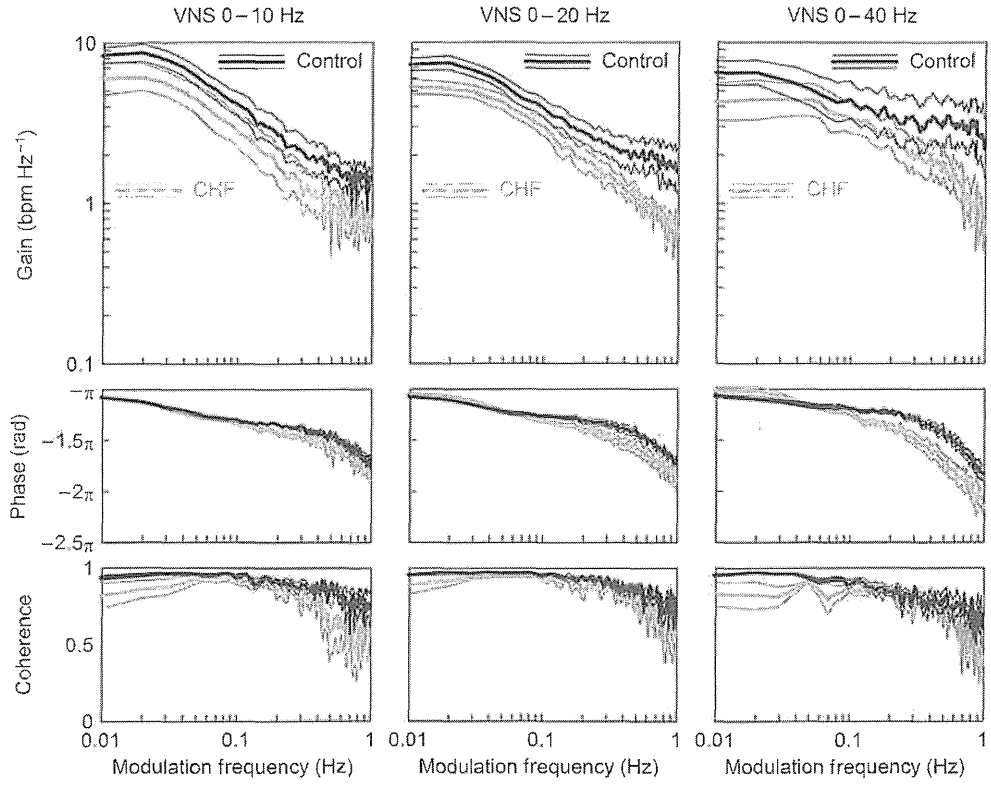

Figure 3 Group-averaged transfer functions from vagal nerve stimulation (VNS) to heart rate obtained from the control group (black lines) and the chronic heart failure (CHF) group (grey lines). The thick and thin lines indicate mean and mean ± SE respectively.

(1971) termed the phenomenon that the vagal control of HR is augmented by concomitant sympathetic activation as accentuated antagonism. In a present study, changes in efferent sympathetic nerve activity were minimized within individual animals by disabling the baroreflexes. However, it is plausible that the CHF group had higher basal sympathetic tone than the control group (Riegger 1985). While the accentuated antagonism does not conform to the attenuation of the steady-state gain, the presynaptic inhibition might have contributed to the attenuation of the steady-state gain in the CHF group.

Effects of CHF and VNS rate on the relative HF gain

The relative HF gain, R, modifies the transduction property of dynamic gain in the higher frequencies (Fig. 4b, top). An increase in the relative HF gain reduces the phase delay (Fig. 4b, middle) and enhances the initial drop seen in the step response of HR (Fig. 4b, bottom). A new finding of the present study is the augmentation in the relative HF gain with increasing the VNS rate, as evidenced by the positive B_{VNS} on the relative HF gain (Table 2). Furthermore, the effect of VNS rate on the relative HF gain was totally cancelled by the interaction effect (the negative $B_{Interaction}$ with approximately the same absolute value as the positive B_{VNS}), indicating that the increase in the VNS rate did not augment the relative HF gain in the CHF group. It can be interpreted that increasing the VNS rate enhanced the initial drop of the step response of HR in the control rats but not in the CHF rats. A previous study in rabbits has shown that a direct action of acetylcholine through muscarinic potassium (K_{ACh}) channels plays an essential role in the HR control at high VNS rates compared to a cyclic-AMP-mediated indirect pathway (Mizuno *et al.* 2007). Because K_{ACh} channels regulate rapid HR response, it is conceivable that the increase in the VNS rate increased the contribution of K_{ACh} channels, resulting in the augmentation of dynamic gain in the higher frequency range in the control group. The density of K_{ACh} channels and the sensitivity of K_{ACh} channels to G_i-mediated channel activation are reduced in atrial myocytes isolated from failing human hearts compared to donor atria (Koumi *et al.* 1994). The reduced K_{ACh} channel density and sensitivity may lead to the loss of the high VNS rate-induced augmentation in the relative HF gain in the CHF group.

Cerutti *et al.* (1991) defined the HF band in rats to be above 0.75 Hz based on the spectral analysis of

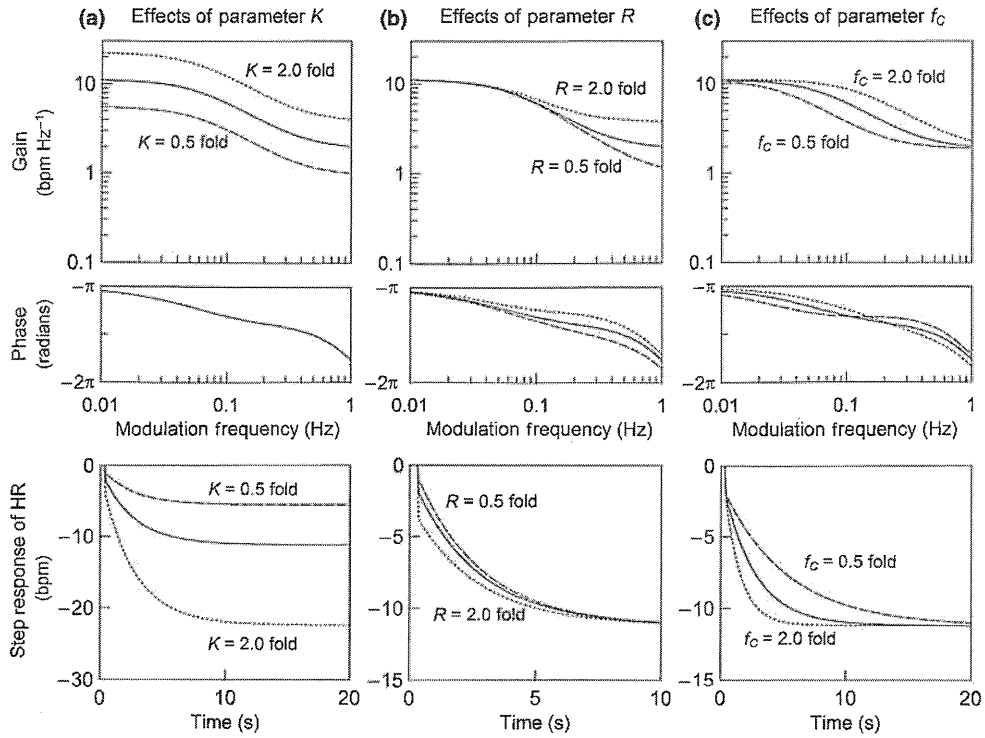

Figure 4 Schematic presentation of the effects of transfer function parameters. Gain plots (top panels), phase plots (middle panels) and step responses of heart rate (HR) derived from the transfer function (bottom panels) are shown. (a) The steady-state gain, K, determines overall responsiveness of HR. (b) The relative high-frequency gain, R, determines the magnitude of initial drop of the HR response. (c) The corner frequency, f_C, determines the rapidness of the HR response. In all panels, the solid lines represent the transfer function and step response derived from 10-Hz vagal nerve stimulation in the control group. The dotted lines indicate the effects of twofold increase in each parameter. The dashed lines indicate the effects of decreasing each parameter to 0.5-fold of the control value.

Table 2 Results of multiple linear regression analysis

	C	B_{VNS}	B_{CHF}	$B_{Interaction}$	R^2
K (bpm Hz^{-1})	8.87 ± 0.42	−0.93 ± 0.32**	−2.31 ± 0.59**	0.04 ± 0.46	0.87
f_C (Hz)	0.050 ± 0.015	0.004 ± 0.012	−0.005 ± 0.022	0.044 ± 0.017*	0.72
L (s)	0.31 ± 0.02	0.04 ± 0.02	0.03 ± 0.03	−0.0002 ± 0.027	0.54
R	0.14 ± 0.04	0.15 ± 0.03**	−0.03 ± 0.06	−0.14 ± 0.04**	0.77
−3 dB point (Hz)	0.042 ± 0.032	0.053 ± 0.025*	0.006 ± 0.046	−0.009 ± 0.035	0.49

K: steady-state gain; f_C: corner frequency; L: pure dead time; R: the ratio of high-frequency gain to the steady-state gain in the transfer function from vagal nerve stimulation (VNS) to heart rate; −3 dB point: the point at which frequency the dynamic gain decreases by 3 dB relative to the steady-state gain; C: constant; B_{VNS}: coefficient for the effect of VNS rate; B_{CHF}: coefficient for the effect of chronic heart failure (CHF); $B_{Interaction}$: coefficient for the interaction between the effects of VNS rate and CHF. *$P < 0.05$ and **$P < 0.01$ by a multiple linear regression analysis.

HRV. In this frequency band, the discrepancy in the dynamic gain between the control and CHF group became magnified during 20- and 40-Hz VNS (Fig. 3). Therefore, the depression of the HF components in CHF can occur due to changes in the dynamic characteristics of the peripheral vagal control of HR even if the vagal outflow from the central nervous system remains unchanged. The upper frequency bound of the HF band was 3.85 Hz (a half of 1/130 ms) in the study by Cerutti *et al.* (1991). In the present study, however, the transfer function was identified only up to 1 Hz. This is because HR decreased as low as 100 bpm (1.66 Hz) during intense VNS (Fig. 1a). If we assume that 1.66 Hz is an effective sampling frequency of the HR signal, the valid upper bound for the spectral calculation becomes 0.83 Hz.

Effects of CHF and VNS rate on the corner frequency

The corner frequency, f_C, determines horizontal location of the transduction property in the gain plot (Fig. 4c, top). The effect of the corner frequency on the phase plot is rather complex due to the presence of relative HF gain (Fig. 4c, middle). An increase in the corner frequency accelerates the step response of HR (Fig. 4c, bottom). The effect on the corner frequency was significantly positive only in the interaction effect ($B_{Interaction}$), suggesting that the increase in the VNS rate increased the corner frequency in the CHF group alone. However, if we calculate the corner frequency based on another definition (the point at which the dynamic gain decreases by 3 dB from the steady-state gain), the effect of VNS rate (B_{VNS}) was significantly positive and the interaction effect became insignificant (Table 2). Berger *et al.* (1989) pointed out that the dynamic gain of the transfer function fell off at a lower frequency when lower mean VNS rates were used, which is consistent with the positive effect of the VNS rate on the −3 dB point. Further studies are required to identify the mechanism for changes in the corner frequency induced by the increase in the VNS rate. Nonlinearity of the HR response may be involved in the changes in the corner frequency, because the coherence values were lower during 40-Hz VNS, especially in the CHF group.

Limitations

Several limitations need to be noticed. Because this study was performed under urethane and α-chloralose anaesthesia and surgical preparation, autonomic tone might have been different from conscious physiological conditions. The anaesthesia and surgical preparation might have also affected the autonomic control of HR. However, because we stimulated the distal end of the sectioned vagal nerve and observed the HR response under the same experimental settings, comparison between the control and CHF groups may be valid.

We have examined three intensities of VNS rate. Although comparing the VNS rate to physiologic levels is difficult, if we assume that physiologic levels of efferent vagal nerve traffic exert a 10% reduction relative to a baseline HR (Mizuno *et al.* 2011), judging from the per cent decrease in mean HR during VNS, 10-Hz VNS may be most relevant in the physiologic sense. The 40-Hz VNS must be interpreted as an extreme case.

Conclusion

We have shown that the dynamic characteristics of the peripheral vagal control of HR differ between the control and CHF groups. In the CHF group, the high VNS rate-induced augmentation in the relative HF gain was not observed. As a result, the dynamic HR response to VNS was significantly depressed in the HF range in the CHF group compared to the control group. In addition to the reduced vagal outflow from the central nervous system and attenuated parasympathetic ganglionic transmission, changes in the dynamic characteristics of the peripheral vagal control of HR may contribute to the manifestation of decreased HF components of HRV observed in CHF. The depression of the HF components does not necessarily indicate the reduced vagal outflow from the central nervous system. The VNS is explored as a replacement treatment of diminished vagal tone in CHF (Li *et al.* 2004, Schwartz 2011). Careful interpretation may be required as to the depression of HF components in CHF if it is used to assess the vagal tone for the selection of possible target patients of the VNS therapy.

Conflict of interest

The authors declare that they have no conflict of interest.

This study was supported by Health and Labour Sciences Research Grants (H19-nano-Ippan-009, H20-katsudo-Shitei-007 and H21-nano-Ippan -005) from the Ministry of Health, Labour and Welfare of Japan; and by the Grant-in-Aid for Scientific Research (C-23592319, 23-01705) promoted by the Ministry of Education, Culture, Sports, Science and Technology of Japan; and by the Industrial Technology Research Grant Program from the New Energy and Industrial Technology Development Organization (NEDO) of Japan.

References

Akselrod, S., Gordon, D., Ubel, F.A., Shannon, D.C., Berger, A.C. & Cohen, R.J. (1981) Power spectrum analysis of heart rate fluctuation: a quantitative probe of beat-to-beat cardiovascular control. *Science* **213**, 220–222.

Berger, R.D., Saul, J.P. & Cohen, R.J. (1989) Transfer function analysis of autonomic regulation. I. Canine atrial rate response. *Am J Physiol Heart Circ Physiol* **256**, H142–H152.

Bibevski, S. & Dunlap, M.E. (1999) Ganglionic mechanisms contribute to diminished vagal control in heart failure. *Circulation* **99**, 2958–2963.

Cerutti, C., Gustin, M.P., Paultre, C.Z., Lo, M., Julien, C., Vincent, M. & Sassard, J. (1991) Autonomic nervous system and cardiovascular variability in rats: a spectral analysis approach. *Am J Physiol Heart Circ Physiol* **261**, H1292–H1299.

Du, X.J., Cox, H.S., Dart, A.M. & Esler, M.D. (1998) Depression of efferent parasympathetic control of heart rate in rats with myocardial infarction: effect of losartan. *J Cardiovasc Pharmacol* **31**, 937–944.

Glantz, S.A. & Slinker, B.K. 2001. *Primer of Applied Regression & Analysis of Variance*, 2nd edn. McGraw-Hill, New York.

Kawada, T., Ikeda, Y., Sugimachi, M., Shishido, T., Kawaguchi, O., Yamazaki, T., Alexander, J. Jr. & Sunagawa, K. (1996) Bidirectional augmentation of heart rate regulation by autonomic nervous system in rabbits. *Am J Physiol Heart Circ Physiol* 271, H288–H295.

Kawada, T., Yamazaki, T., Akiyama, T., Li, M., Zheng, C., Shishido, T., Mori, H. & Sugimachi, M. (2007) Angiotensin II attenuates myocardial interstitial acetylcholine release in response to vagal stimulation. *Am J Physiol Heart Circ Physiol* 293, H2516–H2522.

Kawada, T., Mizuno, M., Shimizu, S., Uemura, K., Kamiya, A. & Sugimachi, M. (2009) Angiotensin II disproportionally attenuates dynamic vagal and sympathetic heart rate controls. *Am J Physiol Heart Circ Physiol* 296, H1666–H1674.

Kawada, T., Li, M., Kamiya, A., Shimizu, S., Uemura, K., Yamamoto, H. & Sugimachi, M. (2010) Open-loop dynamic and static characteristics of the carotid sinus baroreflex in rats with chronic heart failure after myocardial infarction. *J Physiol Sci* 60, 283–298.

Kawada, T., Uemura, K., Shimizu, S., Kamiya, A., Turner, M., Mizuno, M., Sunagawa, K. & Sugimachi, M. (2012) Consideration on parameter determination on a new model describing dynamic vagal heart rate control in rats. *Conf Proc IEEE Eng Med Biol Soc* 2012, 3809–3812.

Koumi, S., Arentzen, C.E., Backer, C.L. & Wasserstrom, J.A. (1994) Alterations in muscarinic K^+ channel response to acetylcholine and to G protein-mediated activation in atrial myocytes isolated from failing human hearts. *Circulation* 90, 2213–2224.

Levy, M.N. (1971) Sympathetic-parasympathetic interactions in the heart. *Circ Res* 29, 437–445.

Li, M., Zheng, C., Sato, T., Kawada, T., Sugimachi, M. & Sunagawa, K. (2004) Vagal nerve stimulation markedly improves long-term survival after chronic heart failure in rats. *Circulation* 109, 120–124.

Miyamoto, T., Kawada, T., Yanagiya, Y., Inagaki, M., Takaki, H., Sugimachi, M. & Sunagawa, K. (2004) Cardiac sympathetic nerve stimulation does not attenuate dynamic vagal control of heart rate via alpha-adrenergic mechanism. *Am J Physiol Heart Circ Physiol* 287, H860–H865.

Mizuno, M., Kamiya, A., Kawada, T., Miyamoto, T., Shimizu, S. & Sugimachi, M. (2007) Muscarinic potassium channels augment dynamic and static heart rate responses to vagal stimulation. *Am J Physiol Heart Circ Physiol* 293, H1564–H1570.

Mizuno, M., Kawada, T., Kamiya, A., Miyamoto, T., Shimizu, S., Shishido, T., Smith, S.A. & Sugimachi, M. (2010) Dynamic characteristics of heart rate control by the autonomic nervous system in rats. *Exp Physiol* 95, 919–925.

Mizuno, M., Kawada, T., Kamiya, A., Miyamoto, T., Shimizu, S., Shishido, T., Smith, S.A. & Sugimachi, M. (2011) Exercise training augments the dynamic heart rate response to vagal but not sympathetic stimulation in rats. *Am J Physiol Regul Integr Comp Physiol* 300, R969–R977.

Nakahara, T., Kawada, T., Sugimachi, M., Miyano, H., Sato, T., Shishido, T., Yoshimura, R., Miyashita, H., Inagaki, M., Alexander, J. Jr. & Sunagawa, K. (1998) Accumulation of cAMP augments dynamic vagal control of heart rate. *Am J Physiol* 275, H562–H567.

Olshansky, B., Sabbah, H.N., Hauptman, P.J. & Colucci, W.S. (2008) Parasympathetic nervous system and heart failure: pathophysiology and potential implications for therapy. *Circulation* 118, 863–871.

Persson, P.B. & Henriksson, J. (2011) Good publication practise in physiology. *Acta Physiol* 203, 403–407.

Riegger, A.J. (1985) Neurohumoral vasoconstrictor systems in heart failure. *Eur Heart J* 6, 479–489.

Sagawa, K. 1983. Baroreflex control of systemic arterial pressure and vascular bed. In: J.T. Shepherd & F.M. Abboud, (eds) *Handbook of Physiology, Sect 2, The Cardiovascular System, Vol III, Peripheral Circulation and Organ Blood Flow*, pp. 453–496. Am Physiol Soc, Bethesda, MD.

Sato, T., Kawada, T., Miyano, H., Shishido, T., Inagaki, M., Yoshimura, R., Tatewaki, T., Sugimachi, M., Alexander, J. Jr. & Sunagawa, K. (1999) New simple methods for isolating baroreceptor regions of carotid sinus and aortic depressor nerves in rats. *Am J Physiol Heart Circ Physiol* 276, H326–H332.

Schwartz, P.J. (2011) Vagal stimulation for heart diseases: from animals to men. – An example of translational cardiology. *Circ J* 75, 20–27.

Shoukas, A.A., Callahan, C.A., Lash, J.M. & Haase, E.B. (1991) New technique to completely isolate carotid sinus baroreceptor regions in rats. *Am J Physiol Heart Circ Physiol* 260, H300–H303.

Task Force of the European Society of Cardiology, the North American Society of Pacing and Electrophysiology (1996) Heart rate variability: standards of measurement, physiological interpretation and clinical use. *Circulation* 93, 1043–1065.

Wetzel, G.T., Goldstein, D. & Brown, J.H. (1985) Acetylcholine release from rat atria can be regulated through an α_1-adrenergic receptor. *Circ Res* 56, 763–766.

Appendix A mathematical model for the transfer function from VNS to HR in rats

The newly proposed transfer function model has a degree of freedom sufficient to describe the transfer function from VNS to HR observed in the present study. The fitting was performed in the frequency domain to minimize the following error function (Kawada *et al.* 2012).

$$\mathrm{err} = \sum_{k=1}^{N} \frac{1}{k} |\log[H(f_k)] - \log[M(f_k)]|^2$$

$$f_k = f_0 \times k$$

where log indicates a complex logarithmic function, f_0 is the fundamental frequency of the Fourier transformation, k is the index of frequency, and f_k is the k-th frequency. $H(f_k)$ and $M(f_k)$ are the estimated and model transfer functions respectively. This error function allows simultaneous approximation of gain and phase. N indicates the number of data points to fit and was set to 102 to approximate the transfer function up to 1 Hz.

J Pharmacol Sci 121, 1 – 8 (2013)

Journal of Pharmacological Sciences

Full Paper

Effects of an hERG Activator, ICA-105574, on Electrophysiological Properties of Canine Hearts

Mahoko Asayama[1,2], Junko Kurokawa[1,*], Kiyoshi Shirakawa[2], Hisashi Okuyama[2], Toshiki Kagawa[2], Jun-ichi Okada[3], Seiryo Sugiura[3], Toshiaki Hisada[3], and Tetsushi Furukawa[1]

[1]*Department of Bio-informational Pharmacology, Medical Research Institute, Tokyo Medical and Dental University, 1-5-45 Yushima, Bunkyo-ku, Tokyo 113-8510, Japan*

[2]*Safety Evaluation Research Laboratories, Research Division, Mitsubishi Tanabe Pharma Corporation, Tokyo 103-8405, Japan*

[3]*Graduate School of Frontier Sciences, the University of Tokyo, Chiba 277-8563, Japan*

Received October 3, 2012; Accepted October 29, 2012

Abstract. In short QT syndrome, inherited gain-of-function mutations in the human *ether a-go-go-related* gene (hERG) K^+ channel have been associated with development of fatal arrhythmias. This implies that drugs that activate hERG as a side effect may likewise pose significant arrhythmia risk. hERG activators have been found to have diverse mechanisms of activation, which may reflect their distinct binding sites. Recently, the new hERG activator ICA-105574 was introduced, which disables inactivation of the hERG channel with very high potency. We explored characteristics of this new drug in several experimental models. Patch clamp experiments were used to verify activation of hERG channels by ICA-105574 in human embryonic kidney cells stably-expressing hERG channels. ICA-105574 significantly shortened QT and QTc intervals and monophasic action potential duration (MAP_{90}) in Langendorff-perfused guinea-pig hearts. We also administered ICA-105574 to anesthetized dogs while recording ECG and drug plasma concentrations. ICA-105574 (10 mg/kg) significantly shortened QT and QTc intervals, with a free plasma concentration of approximately 1.7 μM at the point of maximal effect. Our data showed that unbound ICA-105574 caused QT shortening in dogs at concentrations comparable to the half maximal effective concentration (EC_{50}, 0.42 μM) of hERG activation in the patch clamp studies.

Keywords: hERG activator, QT and QTc interval, KCNH2, I_{Kr} channel, pro-arrhythmia

Introduction

The rapid delayed rectifier K^+ channel current (I_{Kr}) conducted by the human *ether a-go-go-related* gene (hERG, now termed KCNH2) channel is a major contributor to repolarization of the cardiac action potential (1). Loss-of-function mutations in hERG are associated with long QT syndrome (type LQT-2), which is a syndrome characterized by prolonged QT intervals on the electrocardiogram (ECG) and a ventricular tachycardia called torsades de pointes (TdP) (1, 2). There is an acquired form of long QT syndrome typically caused by blockade of I_{Kr} by commonly prescribed drugs, which can result in serious consequences including lethal arrhythmias and/or cardiac sudden death (3). In contrast, little is known about the consequences of enhanced activation of the hERG channel, whether induced by genetic mutations or by pharmacological intervention. A form of inherited short QT syndrome (SQT-1) associated with a gain-of-function mutation in the hERG channel was first reported in 2004 (4). At the cellular and tissue level, hERG activators have been employed to simulate SQT-1 and explore the cellular basis for its arrhythmogenesis. Based on structure–action-relationship analysis of hERG channels, previous hERG activators can be classified into at least two types. The drug RPR260243 binds to residues located near the intracellular end of the S5 and S6 transmembrane segments of the hERG channel and augments I_{Kr} currents by a dual mechanism of slowed deactivation and attenuated P-type inactivation. Alternatively, PD-

*Corresponding author. junkokuro.bip@mri.tmd.ac.jp
Published online in J-STAGE on December 14, 2012 (in advance)
doi: 10.1254/jphs.12220FP

118057 binds to the pore helix and the nearby S6 segment and enhances I_{Kr} currents by attenuating inactivation with little effect on deactivation.

Recently the organic chemical compound ICA-105574 was introduced as a new type of hERG activator (5). Mutagenesis study (6) revealed that the molecular determinant of the binding site was distinct from those of RPR260243 and PD-118057, but had some overlap with them. ICA-105574 shifts the voltage dependence of P-type inactivation to a very positive direction and removes the hERG channel from inactivation at physiological membrane potentials. Although the first report for ICA-105574 (5) showed shortening of action potential duration (APD) in guinea-pig ventricular myocytes, consequences of hERG activation by ICA-105574 in vivo have not been studied. Thus, the goal of the present study was to investigate the effects of ICA-105574 on ECG parameters and monophasic action potentials (MAP) obtained from Langendorff-perfused guinea-pig hearts and anesthetized dogs. In the canine experiments, free drug plasma concentrations were estimated from drug plasma concentrations.

Materials and Methods

Patch-clamp experiments

Patch-clamp experiments were conducted as described previously (7). Briefly, human embryonic kidney (HEK) 293 cells stably expressing the hERG channel (Merck Millipore, Tokyo) were cultured in Minimum Essential Medium supplemented with 10% FBS and 0.5 mg/mL geneticine. hERG channel currents were recorded at room temperature (23°C – 25°C) using the whole-cell patch clamp technique with an Axopatch 200B amplifier (Molecular Devices, Sunnyvale, CA, USA). The control bath solution contained 137 mM NaCl, 4 mM KCl, 1.8 mM $CaCl_2$, 1 mM $MgCl_2$, 10 mM glucose, and 10 mM HEPES, pH 7.4. The drugs were added to the bath solution. Borosilicate glass pipettes (2 – 5 MΩ resistance) were filled with an internal solution containing 130 mM KCl, 1 mM $MgCl_2$, 5 mM EGTA, 5 mM MgATP, and 10 mM HEPES, pH 7.2. Series resistance was 3 – 6 MΩ. Signals were filtered at 5 kHz, sampled at 10 kHz, and compensated for cell capacitance but not series resistance. Unless otherwise noted, hERG currents were elicited at 0.1 Hz with 2-s activating pulses to 10 mV (Vt) followed by 2-s pulses of −50 mV from a holding potential of −80 mV. To obtain concentration–response relationships, the peak current amplitudes at Vt were monitored until current magnitude reached a steady-state level before and after administration of drugs at each concentration. Clampex 9.2 or 10.1 software (Molecular Devices) was used to acquire and analyze data.

Animals

All experiments were performed according to the "Rules for Feeding and Storage of Experimental Animals and Animal Experiments" and approved by the Institutional Animal Care and Use Committee of Mitsubishi Tanabe Pharma Corporation.

ECG and MAP in Langendorff-perfused guinea-pig hearts

ECG and MAP were measured using the previously reported method (8). Hearts were dissected from male Hartley guinea pigs (body weight 380 – 650 g; Japan SLC, Inc., Shizuoka) anesthetized with sodium pentobarbital (50 mg/kg, i.p.; Kyoritsu Seiyaku Co., Tokyo), mounted on a Langendorff apparatus and perfused at approximately 80 mmHg with an aerated Krebs-Henseleit solution. Experiments were carried out with solution temperatures at 37°C ± 0.5°C. Two electrodes were placed, one at the apex of the heart and the other in the aortic cannula, to generate bipolar ECG. MAP was recorded from the epicardium of the left ventricular surface. The right ventricle was paced at approximately 2.5 times the threshold voltage by an electronic stimulator (Fukuda Denshi, Tokyo) via a bipolar electrode attached to its surface. Signals were amplified with differential amplifiers (DAM50 system; World Precision Instruments, Sarasota, FL, USA) and sampled at 1 kHz. Data were acquired and analyzed with WinVAS3 software (Ver. 1.1, Physio-Tech, Tokyo). Corrected QT intervals (QTc) were calculated using three different formulas, Van de Water's [QTc (V) = QT − 0.087 (RR − 1000)] (9), Bazett's [QTc (B) = $QT/RR^{1/2}$] (10), and Fridericia's formula [QTc (F) = $QT/RR^{1/3}$] (11). In MAP recordings, the APD at the 90% repolarization level was defined as MAP_{90}. To stabilize sinus rhythm beating, hearts were perfused for more than 60 min before experimental protocols were started. The evaluation protocol consisted of 20-min perfusion of vehicle [0.1% (v/v) dimethylsulphoxide, DMSO] as the control, followed by cumulative additions of ICA-105574 at final concentrations of 0.3, 1, and 3 μM (20-min perfusion for each). A vehicle only protocol was also run as a time-matched control. Parameters of ECG and MAP were evaluated at the end of each 20-min perfusion. In addition, MAP_{90} was determined under pacing at 300 beats/min (bpm), a rate far above the spontaneous sinus rate. The pacing was also applied at the end of each 20-min perfusion period.

ECG recordings in anesthetized dogs

Surface lead II ECG was measured in four anesthetized male beagles (body weight, 11 – 17 kg) as described previously (12). The dogs were anesthetized initially with 30 mg/kg sodium thiopental, i.v. (Mitsubishi Tanabe

Pharma, Osaka) and maintained in the anesthetized condition with inhalation of 1% halothane (Takeda Chemical Industries, Osaka). The ECG data were acquired with a polygraph system (RM-6000; Nihon Kohden, Tokyo) and recorded on graph paper as well as onto a computer at 1 kHz. Data analysis was performed with software WinVAS3 Ver1.1 (Physio-Tech, Tokyo) or manually using calipers. The ECG parameters studied were spontaneous heart rate, QRS duration, PR, QT, and QTc intervals. ICA was administered at two doses, 1 and 10 mg/kg, as a 10-min intravenous infusion every 30 min and compared with vehicle-only infusion. In two of the four dogs, a 3 mg/kg dose was studied as well. Each ECG parameter was evaluated before the start of infusion and at 5, 10, 15, 20, and 30 min after the start of infusion at each dose. In addition, at the highest dose of 10 mg/kg ICA-105547, ECG parameter evaluation was extended to include the time points 45 and 60 min after the start of the infusion.

Analytic determination of drug exposure

Plasma concentration of the drug was determined in the plasma samples obtained from the same animal in which surface ECG was monitored. Blood was sampled from the femoral vein at 5, 10, 20, and 30 min after the start of drug infusion and additionally at 60 min for the highest dose. The plasma was collected from the supernatant of blood samples except for the vehicle sample after centrifugation at 1500 *g* for 30 min at 4°C and stored at −80°C until the drug concentration was measured. Plasma concentration of ICA-105574 was determined by HPLC (Agilent 1200, Agilent Technologies or CLASS-VP, Shimadzu, Kyoto) and MS/MS (API 3000 or API 5000; AB SCIEX, Foster City, CA, USA). The protein binding ratio of ICA-105574 in canine plasma was determined by a micro-scale ultracentrifugation method (13) using UPLC/MS/MS (Waters, Milford, MA, USA). Estimated free drug plasma concentrations were calculated using the results of the protein binding ratio (98.8%).

Statistics

All values are presented as the mean ± S.E.M. Graphical and statistical analysis were carried out using Origin 8.0J (Microcal, Northampton, MA, USA) or SAS (SAS 9.1.3, SAS Institute, Cary, NC, USA), respectively. Statistical significance was assessed with Student's *t*-test for paired comparisons and adjusted by a Bonferroni method for multiple comparisons, unless otherwise noted. Time-dependent effects of ICA were analyzed in each group using one-way repeated measures ANOVA with the time as the factor of the analysis, followed by a Bonferroni post hoc test. Differences with P value < 0.05 were considered to be significant.

Chemicals

ICA-105574 was synthesized by the Medicinal Chemistry Research Laboratories of Mitsubishi Tanabe Pharma Co. In the in vitro and ex vivo experiments, ICA-105574 was dissolved with DMSO (Sigma-Aldrich, St. Louis, MO, USA) as a stock solution and diluted with bath solution or Krebs-Henseleit solution just before use. The final concentration of DMSO in test solutions was 0.1% (v/v). For the in vivo experiments, ICA-105574 was dissolved with vehicle (10% *N*,*N*-dimethylacetoamide; Kanto Chemical Co., Inc., Tokyo), 70% polyethylene glycol 400 (Wako Pure Chemical Industries, Ltd., Osaka), and 20% water for injection (Otsuka Pharmaceutical Factory, Inc., Tokushima) up to 10 mg/mL.

Results

ICA-105574 increased hERG currents during the depolarization step

Figure 1 confirms that ICA-105574 synthesized by us activated hERG currents as described previously (5). ICA-105574 enhanced the hERG currents during test pulses to 10 mV in a concentration-dependent manner. The EC_{50} value was estimated as 0.42 ± 0.04 μM with a Hill coefficient (n_H) of 2.5 ± 0.3. The maximal increase in current amplitude (E_{max}) for ICA-105574 was 5.5 ± 0.3–fold greater than the control current. ICA-105574 had little effect on the peak tail currents at −50 mV (Fig. 1A) and at −120 mV (Fig. 1B), and it slowed deactivation as described previously (5).

Analysis of the I-V relationship (Fig. 1B) showed that ICA-105574 enhanced peak hERG currents at test voltages (Vt) more positive than −50 mV (5). Under control conditions, the I-V relationships produced a bell-shape curve (maximal at 0 mV) which reflects the inward rectification of hERG channels resulting from slow activation and fast inactivation (14, 15). ICA-105574 at 2 μM significantly enhanced peak hERG currents at Vt greater than −50 mV and abolished the inward rectification, suggesting that the P-type inactivation was progressively shifted to positive potentials as previously reported (5). As a result, the relative increase in peak currents induced by the activator was more significant at very positive Vt higher than 10 mV. This result implies that ICA-105574 enhances outward cationic currents during the plateau phase of the action potential, resulting in acceleration of ventricular repolarization and shortening of APD.

QT shortening effects of ICA-105574 in guinea pigs

We tested whether ICA-105574 affected ECG and MAP in guinea-pig Langendorff hearts (Fig. 2). ECG or

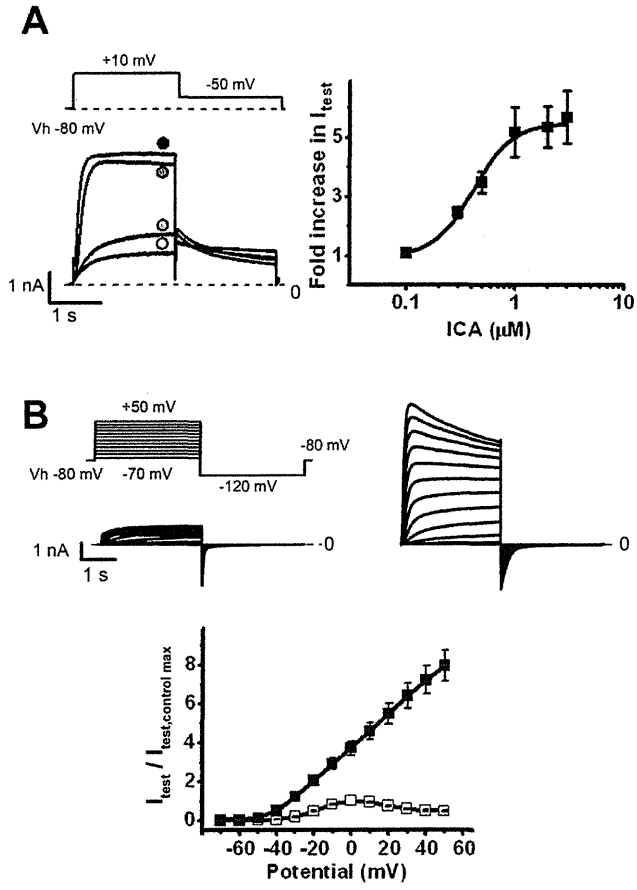

Fig. 1. Effects of ICA-105574 on hERG currents recorded from HEK293 cells stably expressing hERG. A: Concentration-dependent activation of hERG currents by ICA-105574 elicited by 10-mV test pulses (−50 mV return) from a holding potential of −80 mV as indicated above the traces. Shown are representative traces (left) in the absence (control; open circle) and presence of ICA-105574 (0.3 μM: light gray circle, 1 μM: dark gray circle, 3 μM: black circle) and a concentration-dependent curve of hERG activation (right). Plots show the mean ± S.E.M. of peak amplitudes at the test pulses (I_{test}) normalized to control amplitudes before the application of ICA-105574 (n = 5 – 7). Two or three concentrations were tested in a single cell. The curve represents the best fit of data points with a logistic model of nonlinear regression (EC_{50} = 0.42 ± 0.04 μM, n_H = 2.5 ± 0.3). B: Effects of ICA-105574 at 2 μM on the I-V relationship of hERG currents. Membrane currents were elicited by 3-s test pulses to voltages ranging from −70 to +50 mV in 10-mV increments (−120 mV, return) as indicated above the traces. Representative traces in the absence (below voltage protocol) and presence of 2 μM ICA-105574 (upper right) are shown. In the lower panel, the mean ± S.E.M. of normalized amplitude to each maximum amplitude of I_{test} in the absence of the drug are plotted against the test pulse voltages (n = 8).

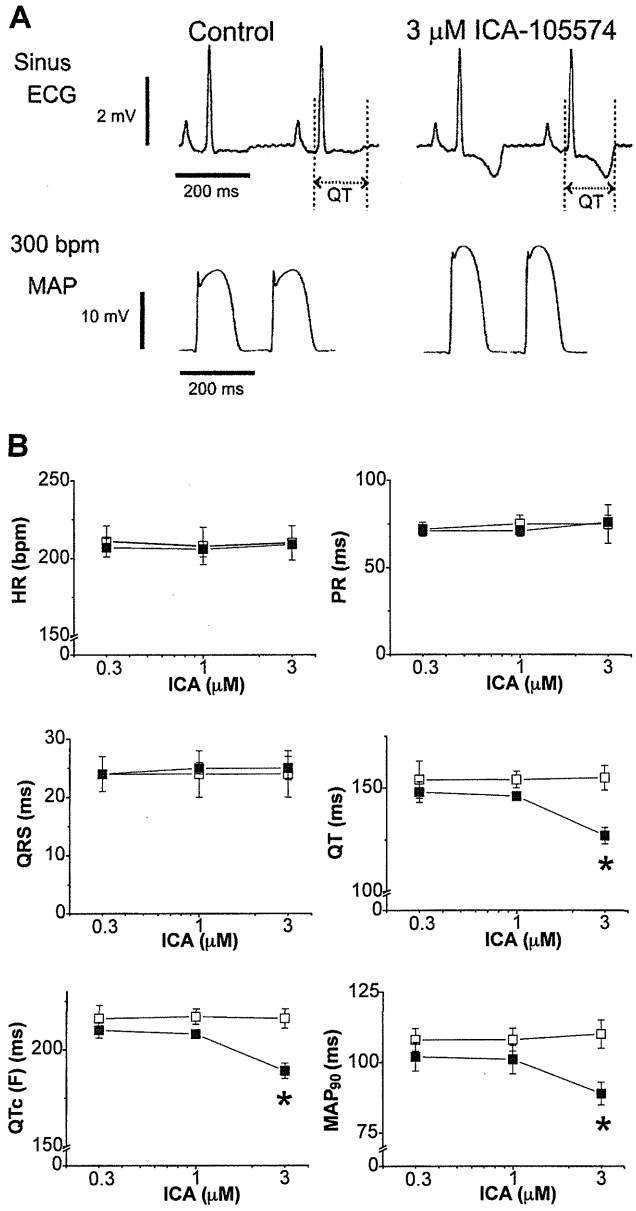

Fig. 2. Effects of ICA-105574 on ECG and MAP recordings from Langendorff perfused guinea-pig hearts. A: Representative ECG and MAP recordings from the same heart pre-treatment (control, left) and after the application of 3 μM ICA-105574 for 20 min (right). Shown are the ECG (upper) during sinus rhythm and MAP_{90} (lower) during ventricular pacing at 300 bpm. B: Effects on ECG parameters and MAP_{90}. ECG parameters after 20-min application of drug (black squares) or vehicle as time-matched control (open squares) were compared to the control value in each heart (n = 5). Error bars represent the S.E.M. PR: PR interval, QRS: QRS width, QT: QT interval, QTc (F): QT interval corrected by the Fridericia formula. *P values < 0.05 according to the unpaired Student's t-test adjusted by Bonferroni's method.

MAP parameters obtained from the Langendorff hearts were stable during vehicle control (0.1% DMSO) perfusion throughout the experiment for more than 80 min. As shown in Fig. 2, at 3 μM, but not at 0.3 or 1 μM, ICA-105574 significantly shortened both QT and QTc (F) intervals and QTc (B) and QTc (V) intervals were as well (data not shown). In addition, MAP_{90} recorded at 300 bpm was also shortened by application of 3 μM ICA-

105574 (P values < 0.05, Student's t-test adjusted by Bonferroni method vs. vehicle control, n = 5). Other ECG parameters such as spontaneous heart rate, PR interval and QRS duration, were not changed. Because the bath solution containing ICA-105574 at concentrations higher than 3 μM produced precipitant in the aerated Krebs-Henseleit solution, we could not increase the concentration to higher than 3 μM.

Effects of ICA-105574 on ECG parameters in anesthetized dogs

To test in vivo effects, we next examined the effects of ICA-105574 on the surface ECG in anesthetized dogs. Typical traces of lead II ECG are shown in Fig. 3A, and the time course of changes in the ECG parameters are plotted in Fig. 3B. Values of ECG parameters are summarized in Table 1. The administration of 1 mg/kg ICA-105574 had no effect on ECG parameters except for an increase in heart rate by 18% of the pre-treatment control (n = 4, $P < 0.05$), similar to that caused by the vehicle (17%, n = 2), probably due to effects of the solvent. Administration of the drug at 3 mg/kg (n = 2) or 1 mg/kg (n = 2) produced no changes. Administration of 10 mg/kg ICA-105574 significantly shortened QT and QTc (V), with a maximal change at 10-min after the start of drug infusion, and significantly increased heart rate by 55% of the pre-treatment control (n = 4, mean from 83 to 121 bpm, $P < 0.01$). The heart rate recorded at 10 mg/kg was higher than that of vehicle (by 17%), indicating that ICA-105574 affected the heart rate at this dose. After infusion of 10 mg/kg ICA-105574 for 5 – 20 min, QTc (V) intervals were maximally shortened by 20% relative to the pre-treatment control, respectively ($P < 0.01$). QTc (B) and QTc (F) intervals were changed as well as QTc (V) (data not shown).

Drug concentration in plasma

The time courses of free plasma concentrations of ICA-105574 are summarized in Fig. 4. The peaks of free drug plasma concentrations were observed at 10-min after the start of infusion (1 mg/kg: 0.16 ± 0.02 μM, n = 4; 3 mg/kg: 0.46 μM, n = 2; and 10 mg/kg: 1.67 ± 0.23 μM, n = 4), corresponding to the time of maximal changes in ECG parameters (Fig. 3).

Discussion

The major finding of this work is that intravenous administration of the novel hERG activator ICA-105574 significantly shortens rate-corrected QT intervals and moderately increases heart rates in anesthetized dogs. This has a major impact on understanding of in vivo effects of hERG activators on cardiac electrophysiology.

A variety of drugs has been reported to cause acquired long QT syndrome through inhibition of the hERG channel. The non-clinical guidance detailed in the International Conference on Harmonization (ICH), S7B suggests that the potential of compounds to interact with I_{Kr} (hERG) and to prolong the QT interval in non-rodent species should be evaluated prior to clinical trials. Compared with the enormous amount of accumulated knowledge on hERG blockers (16), information on the in vivo effects of hERG activators is limited.

At cellular levels, it has been reported that there are at least two types of hERG activators (17). The type 1 activator RPR260243 induces delayed deactivation and a positive shift in the voltage-dependence of inactivation (18, 19). In type 2, PD-118057 (20), its analogue PD-307243 (21), NS1643 (22, 23), and A935142 (24) act primarily to attenuate inactivation. ICA-105574, the drug used in the current study, was initially classified as a type 2 drug because it exhibits a robust depolarizing shift in the voltage dependence of inactivation with modest changes in activation and deactivation (5, 6). Recently, a site-directed mutagenesis study (6) revealed that the binding site on hERG channels for ICA-105574 was distinct from those of RPR260243 (type 1) and PD-118057 (type 2), suggesting that ICA-105574 could be classified as a third type of hERG activator. The binding site for ICA-105574 has overlap with the binding sites of the other two types of activators and with common inhibitors (Y652). Thus, the underlying effects on hERG are expected to vary between classes and between drugs within classes (25).

Selective hERG inhibitors act to delay repolarization and prolong QT intervals on the ECG in vivo at free plasma concentrations comparable to hERG IC_{50}. However, effective potential in vivo is not always comparable to in vitro efficacy for off-target drugs, which have effects on autonomic nervous systems or multiple channels or metabolism, or have indirect effects on the hERG channel such as block of trafficking (16, 26, 27). In the in vivo experiments (Fig. 3), ICA-105574 at a high dose (10 mg/kg) increased heart rates and shortened PR intervals, while ICA-105574 did not affect heart rates and PR intervals in excised Langendorff hearts (Fig. 2). Thus, the autonomic nervous system might be involved in the effects on heart rates and PR intervals possibly by affecting blood pressure (no data). Furthermore, plasma protein binding may affect the effective dose by limiting effective exposure in vivo and should be considered when discussing the correlation between in vitro and in vivo studies. There is little information on this correlation for hERG activators. In the current study, we showed that ICA-105574 shortened QT and QTc intervals in vivo at similar concentrations to which ICA-105574 activates

hERG currents in vitro, suggesting that ICA-105574 is selective for the hERG channel. To our knowledge, this is the first report to show in vivo effects of an hERG-activating compound against validated drug plasma concentrations. The reason that we used anesthetized animals in this study was that stable ECG was obtained continuously under controlled with drug plasma concentrations compared with conscious animals. The halothane probably reduces repolarization reserve through suppression of a slow component of delay rectifiers and the halothane anesthetized dog model has an extent of repolarization thought to be similar to that in healthy human

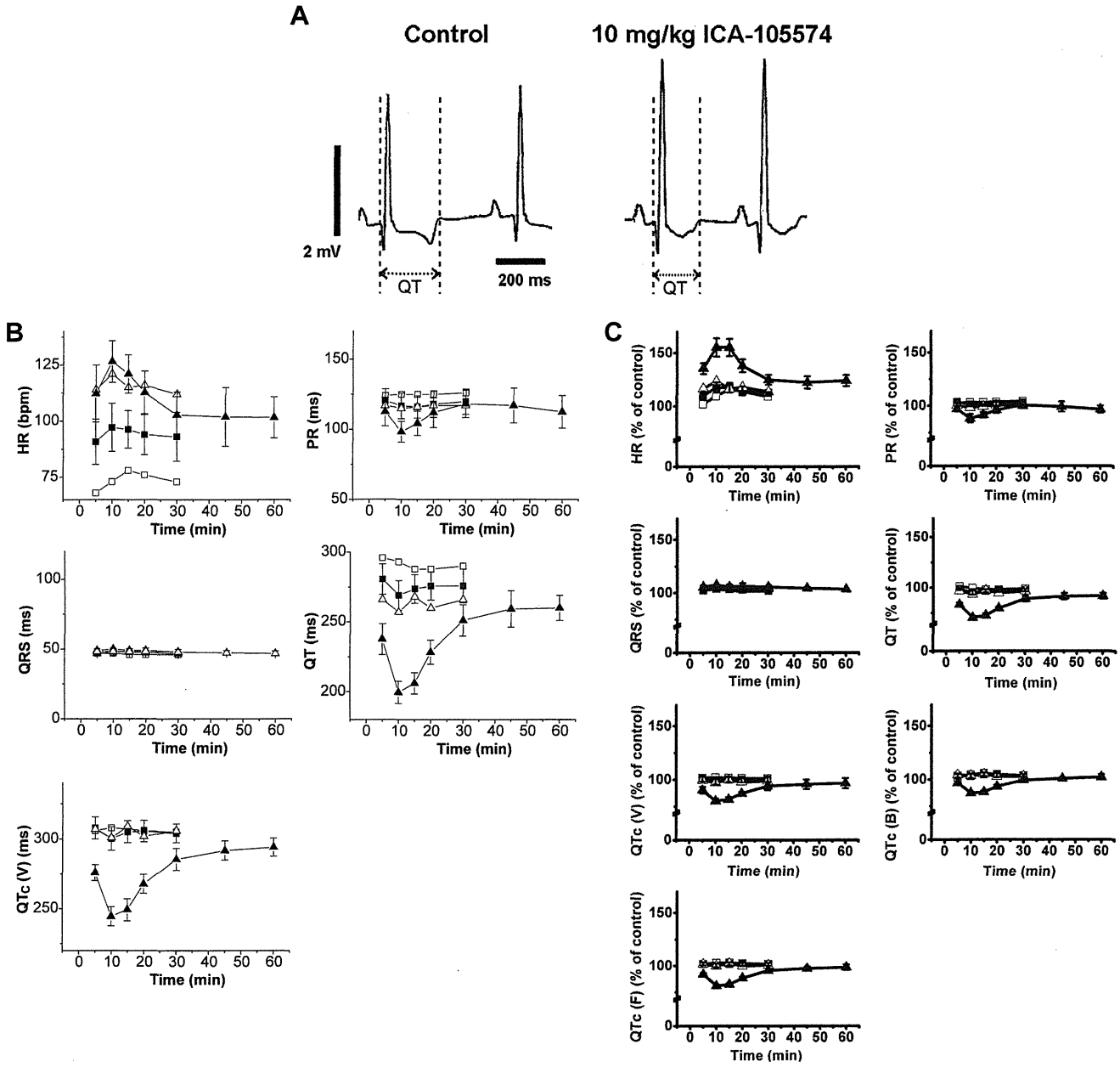

Fig. 3. Effects of ICA-105574 on ECG in anesthetized dogs. A: Shown are representative ECG traces pre-treatment (control) and after 10 mg/kg ICA-105574 intravenous infusion. B: Time-dependent changes in ECG parameters at each time point after vehicle (open squares) or 1 (closed squares), 3 (open triangles), and 10 mg/kg (closed triangles) ICA-105574 administration. Error bars represent the S.E.M. PR: PR interval; QRS: QRS width; QT: QT interval; QTc: corrected QT interval; (V) represent QT interval corrected by Van de Water's formula. The numbers of ECG complexes measured were 4 each for the 1 and 10 mg/kg ICA-105574 administration data and 2 each for the vehicle and 3 mg/kg ICA-105574 administration data. C: Relative changes in ECG parameters in B were calculated by normalizing values of vehicle or ICA-treated to the pre-treatment values in each animal.

Table 1. ECG data of anesthetized dogs

	Control (Pre-treatment)	ICA (1 mg/kg)	ICA (10 mg/kg)	Recovery after ICA (10 mg/kg)
Heart rate (bpm)	83 ± 11	97 ±12*	126 ± 11***	102 ± 11*
PR (ms)	119 ± 8	120 ± 9	105 ± 10*	115 ± 11
QRS (ms)	46 ± 1	47 ± 2	48 ± 2	47 ± 2
QT (ms)	284 ± 12	270 ± 12	200 ± 9***	261 ± 10*
QTc (V) (ms)	305 ± 7	301 ± 10	245 ± 8***	295 ± 8
QTc (B) (ms)	330 ± 15	341 ± 19	288 ± 13***	338 ± 14
QTc (F) (ms)	314 ± 9	315 ± 13	255 ± 10***	310 ± 10

ICA (1 mg/kg), ICA (10 mg/kg): after 10-min infusion of 1 and 10 mg/kg of ICA-105574; Recovery after ICA (10 mg/kg): at 50 min after infusion ended; QTc (V): QT interval corrected for heart rate according to Van de Water formula; QTc (B): QT interval corrected for heart rate according to Bazzett's formula; QTc (F): QT interval corrected for heart rate according to Fridericia formula. Data were expressed as the mean ± S.E.M. *$P < 0.05$, ***$P < 0.001$, one-way ANOVA followed by Bonferroni test vs. control (pre-treatment).

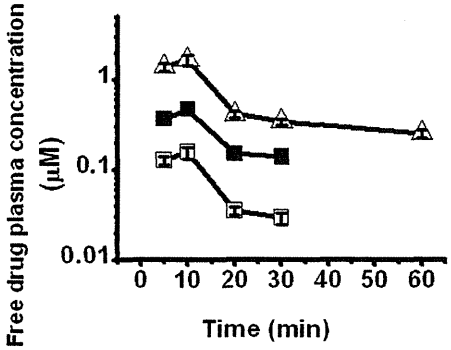

Fig. 4. Estimated free ICA-105574 concentration in canine plasma. The plots show the time course of estimated free ICA-105574 concentration in dog plasma (administration of 1 mg/kg; open squares, 3 mg/kg; closed squares, 10 mg/kg; open triangles). Canine plasma was sampled from the femoral veins of the same dogs in which ECG was measured. Plasma ICA-105574 concentration was determined by the LC/MS/MS method. The protein binding ratio of ICA-105574 in canine plasma was determined by a micro-scale ultracentrifugation method. Estimated free drug plasma concentrations were calculated using the results of this protein binding ratio. All plasma concentrations of ICA-105574 were first obtained as weight concentrations and then converted to molar concentrations (molecular weight, 334.33). The plots were expressed as the mean ± S.E.M. (n = 4) at 1 and 10 mg/kg ICA-105574 and as the mean (n = 2) at 3 mg/kg ICA-105574.

volunteers (28).

As some investigators argued (5), QT shortening by ICA-105574–induced hERG activation might have an impact on the treatment of cardiac arrhythmias associated with long QT intervals, suggesting a potential therapeutic utility of ICA-105574. However, as with the long QT syndromes, the fact that congenital short QT syndromes (29, 30) may lead to susceptibility to arrhythmias raises concerns that QT-shortening drugs could also lead to arrhythmic risk. Although non-clinical data have shown that drug-induced QT and QTc shortening can theoretically lead to ventricular fibrillation and sudden death, the clinical impact of short QT interval is still a matter of debate. The profibrillatory mechanism for short QT is still unclear, although one can speculate that QT shortening causes heterogeneity of repolarization in the heart. Therefore, we have to be careful to use an hERG-channel activator in any patients with electrophysiological disturbances. This study provides an animal model of drug-induced QT shortening caused by hERG activation.

Limitations

Compound solubility issues and the multiple effects of the compound we studied made it more difficult to understand the effects of pure hERG activators in the whole heart.

Therefore, the results were not sufficient to assess our hERG activator's potential for pro-arrhythmia. As a future direction, additional pro-arrhythmic intervention such as extra-pacing or sympathetic nervous stimulations may help to provide evidence for whether hERG activators such as ICA-105574 are pro-arrhythmic or anti-arrhythmic. Because analyzing cardiac dispersion sometimes helps to understand the mechanisms of pro-arrhythmic effects, the data obtained from larger animals, such like dogs in this study, may help provide clues for novel mechanisms.

Acknowledgment

This research was financially supported by the Japan Society for the Promotion of Science (JSPS) through the "Funding Program for World-Leading Innovative R&D on Science and Technology (FIRST Program)" initiated by the Council for Science and Technology Policy (CSTP); Grants from the Ministry of Education, Culture, Sports, Science, and Technology (MEXT) of Japan (23590297 to J.K. and

23390205 to T.F.); and Grants-in-Aid for Scientific Research on Priority Areas (23136503 to J.K.). This work was also supported by a program of support for women researchers from the Tokyo Medical and Dental University. The authors thank Dr. Takekawa and Mrs. Eifuku for measurement of drug plasma concentrations.

References

1 Sanguinetti MC, Jiang C, Curran ME, Keating MT. A mechanistic link between an inherited and an acquired cardiac arrhythmia: HERG encodes the I_{Kr} potassium channel. Cell. 1995;81: 299–307.

2 Clancy CE, Rudy Y. Cellular consequences of HERG mutations in the long QT syndrome: precursors to sudden cardiac death. Cardiovasc Res. 2001;50:301–313.

3 Clancy CE, Kurokawa J, Tateyama M, Wehrens XH, Kass RS. K^+ channel structure-activity relationships and mechanisms of drug-induced QT prolongation. Annu Rev Pharmacol Toxicol. 2003;43:441–461.

4 Brugada R, Hong K, Dumaine R, Cordeiro J, Gaita F, Borggrefe M, et al. Sudden death associated with short-QT syndrome linked to mutations in HERG. Circulation. 2004;109:30–35.

5 Gerlach AC, Stoehr SJ, Castle NA. Pharmacological removal of human ether-a-go-go-related gene potassium channel inactivation by 3-nitro-N-(4-phenoxyphenyl) benzamide (ICA-105574). Mol Pharmacol. 2010;77:58–68.

6 Garg V, Stary-Weinzinger A, Sachse F, Sanguinetti MC. Molecular determinants for activation of human ether-a-go-go-related gene 1 potassium channels by 3-nitro-n-(4-phenoxyphenyl) benzamide. Mol Pharmacol. 2011;80:630–637.

7 Kurokawa J, Tamagawa M, Harada N, Honda S, Bai CX, Nakaya H, et al. Acute effects of oestrogen on the guinea pig and human I_{Kr} channels and drug-induced prolongation of cardiac repolarization. J Physiol. 2008;586:2961–2973.

8 Hamlin RL, Cruze CA, Mittelstadt SW, Kijtawornrat A, Keene BW, Roche BM, et al. Sensitivity and specificity of isolated perfused guinea pig heart to test for drug-induced lengthening of QTc. J Pharmacol Toxicol Methods. 2004;49:15–23.

9 Van de Water A, Verheyen J, Xhonneux R, Reneman RS. An improved method to correct the QT interval of the electrocardiogram for changes in heart rate. J Pharmacol Methods. 1989;22: 207–217.

10 Bazzet H. An analysis of the time relationship of electrocardiograms. Heart. 1920;7:353.

11 Fridericia LS. Die Systolendauer im elektrokardiogramm bei normalen menschen und bei herzkranken. Acta Med Scand. 1920;53:489.

12 Sugiyama A, Hashimoto K. Effects of gastrointestinal prokinetic agents, TKS159 and cisapride, on the in situ canine heart assessed by cardiohemodynamic and electrophysiological monitoring. Toxicol Appl Pharmacol. 1998;152:261–269.

13 Nakai D, Kumamoto K, Sakikawa C, Kosaka T, Tokui T. Evaluation of the protein binding ratio of drugs by a micro-scale ultracentrifugation method. J Pharm Sci. 2004;93:847–854.

14 Schonherr R, Heinemann SH. Molecular determinants for activation and inactivation of HERG, a human inward rectifier potassium channel. J Physiol. 1996;493:635–642.

15 Smith PL, Baukrowitz T, Yellen G. The inward rectification mechanism of the HERG cardiac potassium channel. Nature. 1996;379:833–836.

16 Redfern WS, Carlsson L, Davis AS, Lynch WG, MacKenzie I, Palethorpe S, et al. Relationships between preclinical cardiac electrophysiology, clinical QT interval prolongation and torsade de pointes for a broad range of drugs: evidence for a provisional safety margin in drug development. Cardiovasc Res. 2003; 58:32–45.

17 Perry M, Sanguinetti M, Mitcheson J. Revealing the structural basis of action of hERG potassium channel activators and blockers. J Physiol. 2010;588:3157–3167.

18 Kang J, Chen XL, Wang H, Ji J, Cheng H, Incardona J, et al. Discovery of a small molecule activator of the human *ether-a-go-go-related* gene (HERG) cardiac K^+ channel. Mol Pharmacol. 2005;67:827–836.

19 Perry M, Sachse FB, Sanguinetti MC. Structural basis of action for a human *ether-a-go-go-related* gene 1 potassium channel activator. Proc Natl Acad Sci U S A. 2007;104:13827–13832.

20 Zhou J, Augelli-Szafran CE, Bradley JA, Chen X, Koci BJ, Volberg WA, et al. Novel potent human *ether-a-go-go-related* gene (hERG) potassium channel enhancers and their in vitro antiarrhythmic activity. Mol Pharmacol. 2005;68:876–884.

21 Xu X, Recanatini M, Roberti M, Tseng GN. Probing the binding sites and mechanisms of action of two human *ether-a-go-go-related* gene channel activators, 1,3-bis-(2-hydroxy-5-trifluoromethyl-phenyl)-urea (NS1643) and 2-[2-(3,4-dichloro-phenyl)-2,3-dihydro-1H-isoindol-5-ylamino]-nicotinic acid (PD307243). Mol Pharmacol. 2008;73:1709–1721.

22 Casis O, Olesen SP, Sanguinetti MC. Mechanism of action of a novel human ether-a-go-go-related gene channel activator. Mol Pharmacol. 2006;69:658–665.

23 Hansen RS, Diness TG, Christ T, Demnitz J, Ravens U, Olesen SP, et al. Activation of human ether-a-go-go-related gene potassium channels by the diphenylurea 1,3-bis-(2-hydroxy-5-trifluoromethyl-phenyl)-urea (NS1643). Mol Pharmacol. 2006;69: 266–277.

24 Su Z, Limberis J, Souers A, Kym P, Mikhail A, Houseman K, et al. Electrophysiologic characterization of a novel hERG channel activator. Biochem Pharmacol. 2009;77:1383–1390.

25 Roden DM. Principles in pharmacogenetics. Epilepsia. 2001; 42 Suppl 5:44–48.

26 Shibata S, Okamoto Y, Endo S, Ono K. Direct effects of esmolol and landiolol on cardiac fuction, coronary vasoactivity, and ventricular electrophysiology in guinea-pig hearts. J Pharmacol Sci. 2012;118:255–265.

27 Nishida A, Takizawa T, Matsumoto A, Miki T, Seino S, Nakaya H. Inhibition of ATP-sensitive K^+ channels and L-type Ca^{2+} channels by amiodarone elicits contradictory effect in insulin secretion in MIN6 cells. J Pharmacol Sci. 2011;116:73–80.

28 Takahara A, Sugiyama A, Hashimoto K. Reduction of repolarization reserve by halothane anaesthesia sensitizes the guinea-pig heart for drug-induced QT interval prolongation. Br J Pharmacol. 2005;146:561–567.

29 Bjerregaard P, Nallapaneni H, Gussak I. Short QT interval in clinical practice. J Electrocardiol. 2010;43:390–395.

30 Viskin S, Zeltser D, Ish-Shalom M, Katz A, Glikson M, Justo D, et al. Is idiopathic ventricular fibrillation a short QT syndrome? Comparison of QT intervals of patients with idiopathic ventricular fibrillation and healthy controls. Heart Rhythm. 2004;1: 587–591.

Patient Specific Simulation of Body Surface ECG using the Finite Element Method

JUN-ICHI OKADA, PH.D.,* TERUYOSHI SASAKI, M.SC.,* TAKUMI WASHIO, M.SC.,* HIROSHI YAMASHITA, M.D., PH.D.,† TARO KARIYA, M.D.,† YASUSHI IMAI, M.D., PH.D.,† MACHIKO NAKAGAWA, M.SC.,‡ YOSHIMASA KADOOKA, PH.D.,‡ RYOZO NAGAI, M.D., PH.D.,†,§ TOSHIAKI HISADA, PH.D.,* and SEIRYO SUGIURA, M.D., PH.D.*

From the *Department of Human and Engineered Environmental Studies, Graduate School of Frontier Sciences, The University of Tokyo, Kashiwanoha, Japan; †Department of Cardiovascular Medicine, School of Medicine, The University of Tokyo, Bunkyo-ku, Tokyo, Japan; ‡Fujitsu Ltd., Kawasaki, Kanagawa, Japan; and §Jichi Medical University, Tochigi, Japan

Background: *Recent studies, supported by advances in computer science, have successfully simulated the excitation and repolarization processes of the heart, based on detailed cell models of electrophysiology and implemented with realistic morphology.*

Methods: *In this study, we extend these approaches to simulate the body surface electrocardiogram (ECG) of specific individuals. Patient-specific finite element models of the heart and torso are created for four patients with various heart diseases, based on clinical data including computer tomography, while the parallel multi-grid method is used to solve the dynamic bi-domain problem. Personalization procedures include demarcation of nonexcitable tissue, allocation of the failing myocyte model of electrophysiology, and modification of the excitation sequence. In particular, the adjustment of QRS morphology requires iterative computations, facilitated by the simultaneous visualization of the propagation of excitation in the heart, average QRS vector in the torso, and 12-lead ECG.*

Results: *In all four cases we obtained reasonable agreement between the simulated and actual ECGs. Furthermore, we also simulated the ECGs of three of the patients under bi-ventricular pacing, and once again successfully reproduced the actual ECG morphologies. Since no further adjustments were made to the heart models in the pacing simulations, the good agreement provides strong support for the validity of the models.*

Conclusions: *These results not only help us understand the cellular basis of the body surface ECG, but also open the possibility of heart simulation for clinical applications. (PACE 2013; 36:309–321)*

CRT, computing, electrocardiogram, mapping

Introduction

Recent intense research in cardiac simulation has extended the scope of heart modeling by integrating hierarchical biological components in the heart, ranging from molecules to organs. Development of such a multiscale whole-heart model obviously requires explanation of the different physical principles governing the functional interplay among them.[1,2] With such multiscale, multiphysics features, if successfully implemented, the whole-heart model can be used not only for basic research by extrapolating the knowledge gained at the molecular level and through animal experiments to the behavior of the human heart, but also as a platform for the evaluation of diagnostic tests or the effects of treatment options. However, for the heart models to be truly useful for the latter, that is, for clinical purposes, they must be specific models reproducing the biological characteristics of each patient.

What are the premises for a patient-specific heart model? Although recent diagnostic technologies have provided us with a plethora of data on both morphology and functions to establish and validate the patient-specific heart model, we still consider simulation of the body surface electrocardiogram (ECG) as essential because of its common use in clinical practice as it is less invasive. Furthermore, the important information retrievable from the body surface ECG

This work was supported by the Japan Science and Technology Agency under a grant for Collaborative Development of Innovative Seeds-Practicability Verification Stage, and the Japan Society for the Promotion of Science (JSPS) through its "Funding Program for World-Leading Innovative R&D on Science and Technology (FIRST Program)."

Address for reprints: Jun-ichi Okada, Ph.D., #381 Environmental Building, Kashiwa Campus, The University of Tokyo 5-1-5 Kashiwanoha, Kashiwa, Chiba 277-8563, Japan. Fax: 81-04-7136-4668; e-mail: okada@sml.k.u-tokyo.ac.jp

Received May 17, 2012; revised September 22, 2012; accepted October 23, 2012.

doi: 10.1111/pace.12057

has recently been revisited.[3] In fact, many attempts simulating the ECG based on either a mono- or bi-domain formulation of the cell model for cardiac electrophysiology implemented in image-based models of animal and human hearts have been reported,[4–6] though relatively few studies combine these heart models with an image based torso with various organs segmented to reproduce a realistic ECG.

The major reason for eliminating a realistic torso model from the ECG analysis is the computational cost inherent in such large-scale simulation. Researchers have circumvented this problem by using the boundary element method (BEM) either with the torso (thorax) as the isotropic volume conductor[7,8] or with a realistic torso model using the two step approach. In this approach, *a priori* obtained electrical activity of the heart is mapped onto a coarse torso model and the body surface potential is calculated using either the approximate transfer matrix[5] or a finite element solution.[9] Despite detailed discussion of the convergence and accuracy of these methods,[5,7] we are still unsure whether such approaches ensure clinically approved accuracy for diseased individuals with complex anatomy of both the thorax and heart accompanied by highly variable modes of cardiac excitation and repolarization.

Recently, we developed a method to simulate the human body surface ECG using image-based finite element models of the ventricles and torso, in which various organs are segmented.[10] By applying a multilevel solution technique to a composite mesh consisting of a fine mesh for the heart and a coarse mesh for the torso regions,[11] we solved the large-scale dynamic bi-domain problem in a computationally efficient manner. In the study, we applied this technique to the patient-specific simulation of the body surface ECG. Although the number of subjects studied was small, we were able to successfully reproduce the body surface ECGs for patients under various diseased conditions, thereby showing the potential of this technique for clinical application in the future.

Method

In this study, the clinical data of patients were analyzed retrospectively. The study conformed to the standards set by the latest revision of the *Declaration of Helsinki*, and the protocol was approved by the Ethics Committee of The University of Tokyo. Informed consent was obtained from all patients regarding the use of their clinical data.

Study Subjects

Four patients whose laboratory data, including computer tomography (CT) scans, were available were involved in this study. Profiles of the subjects are given in Table I. Patient #1 had an episode of chest pain, but the clinical investigation revealed no signs of organ abnormalities, and thus he was considered normal. The other three patients suffered from severe congestive heart failure and had undergone implantation of dual chamber pacemakers for cardiac resynchronization therapy (CRT). For these two patients, the data before and after the CRT were analyzed.

Table I.

Patient Characteristics

Patient #	Sex	Age	Diagnosis
1	M	62	chest pain
2	M	73	OMI, p-CABG, CLBBB, CHF, p-CRT
3	M	65	HCM (dilated phase), CHF, p-CRT
4	M	26	AR (p-AVR), CHF, Marfan syndrome susp

OMI = old myocardial infarction; p-CABG = status after cardiac artery bypass graft; CLBBB = complete left bundle branch block; CHF = congestive heart failure; p-CRT = status after the implantation of cardiac resynchronization therapy device; HCM = hypertrophic cardiomyopathy; AR = aortic regurgitation; p-AVR = status after aortic valve replacement; susp: suspect of.

Finite Element Model

Details of finite element models of the human heart and torso have previously been reported.[10,11] As in these previous studies, only the ventricles were modeled and the human ventricular myocyte model of electrophysiology by Ten Tusscher et al. was adopted.[12,13] In addition to the three cell types, that is, endocardial, M-, and epicardial cells, a Purkinje network with high conduction velocity was modeled on the endocardial surface. The average size of each element of the heart model was 0.4 mm but, due to the dilatation of the diseased hearts, the number of elements ranged from 25,067,520 to 64,000,000. We mapped the fiber orientation to each model. However, because there is no available technique for measuring the fiber orientation of beating hearts, we applied the same orientation obtained from the literature (http://gforge.icm.jhu.edu/gf/project/dtmri_data_sets/). For patient #3, a CT scan was performed only for the heart region, and thus a part of the thorax on the right hand side was excluded. Because no deformity was found on the chest X-ray, we constructed the torso model by substituting the missing part with a mirror image of the left hand side of the chest.

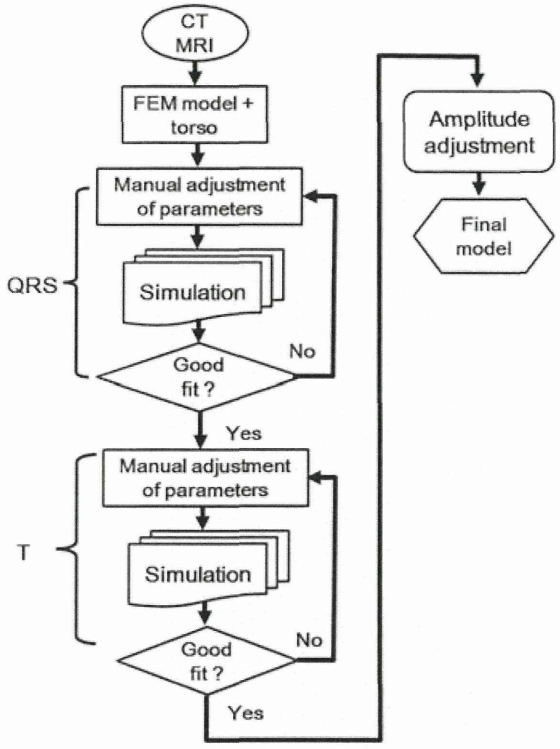

Figure 1. *Workflow showing the simulated ECG fitted to the actual ECG. We adopted a stepwise strategy to sequentially adjust QRS complexes, T waves, and their amplitudes.*

Patient Specific Adjustments to the Model

Patient specific adjustments were made to these models in three steps (Fig. 1). First, we mapped the infarcted region identified by the Tl scintigram where applicable. The region of the permanent defect in perfusion was demarcated and projected onto the heart model as an area of transmural infarction, lacking electrical activity (nonexcitable tissue). However, because Tl scintigram (SPECT) data only provide a coarse map of the infarcted region, we made minor changes to the initially mapped region during ECG matching. In this study, the gray zone between the nonischemic and infarcted region was not considered, owing to the low spatial resolution of the scintigram.

In a previous study, we found that variations in the distribution of cell types with different action potential duration (APD) either in the transmural or apico-basal direction do not change the QRS morphology appreciably (see Fig. 4 in Okada et al.[10]). Accordingly, in the next step, we adjusted the QRS morphology prior to adjusting the distribution of these cell types. Starting from the baseline morphology of the conduction system, which realizes a normal sequence of excitation,[10,14] we shifted the earliest sites of excitation on the endocardium by modifying the distribution of the free-running part of the conduction system to find optimal sites for each patient. To facilitate this procedure, we calculated the instantaneous depolarization (QRS) vector (depicted by arrows in the time-lapse images of the torso in Fig. 3) as the sum of the local excitation vectors in the heart (depicted by small arrows in the time lapse images of the heart in Fig. 2) and simultaneously visualized these in the torso and heart models, respectively (see also the supplementary movie S1). By interactively considering the relationship between the excitation propagation in the heart and the accompanying changes in magnitude and direction of the depolarization vector at any desired moment via the guidance of simultaneously visualized ECGs, the optimal sequence of excitation could be estimated in an efficient manner. Third, the distribution of different cell types was adjusted to reproduce the patient specific T-wave morphologies. Again, for a normal heart, the cell distribution identified in our previous study[10] was applied. The adjustment strategy for a failing heart was based on the two studies. Recently, Glukhov et al. reported that while myocytes with a long APD, presumably M cells, are clustered on the endocardial side in normal human ventricles, such heterogeneity in the APD disappeared in a failing myocardium.[15] Accordingly, for a diseased myocardium, we allocated a single type of failing myocyte model proposed by Winslow et al.,[16] in which the reduction of IK1 and Ito currents, down regulation of the SR Ca^{2+}-ATPase, and up regulation of the Na^{+}-Ca^{2+} exchanger were introduced. The region of the failing myocardium was adjusted according to the patient ECG.

Finally, the thickness of the subcutaneous fat tissue was adjusted to optimize the amplitudes of the ECG waves if necessary.

To facilitate the evaluation of agreement, we also calculated the cross-correlation ($-1 \leq R_{NCC} \leq 1$) between the simulated and actual ECG using the following equation

$$R_{NCC} = \frac{\sum_{j=1}^{12}\sum_{i=1}^{N} A(i,\ j) \times B(i,\ j)}{\sqrt{\sum_{j=1}^{12}\sum_{i=1}^{N} A(i,\ j)^2 \times \sum_{l=1}^{12}\sum_{k=1}^{N} B(k,\ l)^2}},$$

where *A(i,j)* and *B(i,j)* are the voltages at time *i* for the simulated and real ECGs with summation over 12 leads ($j = 1$ to 12). Evaluations were carried out for QRS complexes and entire waves.